Experiments in Fluids 33 (2002) 143–159
DOI 10.1007/s00348-002-0485-9

Experimental studies on particle behaviour and turbulence modification in horizontal channel flow with different wall roughness

J. Kussin, M. Sommerfeld

Abstract Detailed measurements in a developed particle-laden horizontal channel flow (length 6 m, height 35 mm, the length is about 170 channel heights) are presented using phase-Doppler anemometry for simultaneous determination of air and particle velocity. The particles were spherical glass beads with mean diameters in the range of 60 μm–1 mm. The conveying velocity could be varied between about 10 m/s and 25 m/s, and the particle mass loading could reach values of about 2 (the mass loading is defined as the ratio of particle to gas phase mass flow rates), depending on particle size. For the first time, the degree of wall roughness could be modified by exchanging the wall plates. The influence of these parameters and the7 effect of inter-particle collisions on the profiles of particle mean and fluctuating velocities and the normalised concentration in the developed flow were examined. It was shown that wall roughness decreases the particle mean velocity and enhances fluctuating velocities due to irregular wall bouncing and an increase in wall collision frequency, i.e. reduction in mean free path. Thereby, the larger particles are mainly more uniformly distributed across the channel, and gravitational settling is reduced. Both components of the particle velocity fluctuation were reduced with increasing mass loading due to inter-particle collisions and the momentum loss involved. Moreover, the effect of the particles on the air flow and the turbulent fluctuations was studied on the basis of profiles in the developed flow and turbulence spectra determined for the streamwise velocity component. In addition to the effect of particle size and mass loading on turbulence modulation, the influence of wall roughness was analysed. It was clearly shown that increasing wall roughness also results in a stronger turbulence dissipation due to two-way coupling.

Received: 1 February 2002 / Accepted: 1 May 2002
Published online: 18 June 2002

J. Kussin, M. Sommerfeld (✉)
Institut für Verfahrenstechnik,
Fachbereich Ingenieurwissenschaften,
Martin-Luther-Universität Halle-Wittenberg,
06099 Halle (Saale), Germany
E-mail: martin.sommerfeld@iw.uni-halle.de

The research project was financially supported by the Deutsche Forschungsgemeinschaft. This support under contract number So 204/12-1 and 2 is gratefully acknowledged.

1 Introduction

Confined gas–solid flows are frequently found in industrial and chemical process technology. As a result of the complex micro-physical phenomena affecting the particle motion, such as turbulent dispersion, wall collisions, inter-particle collisions and flow modulation by the particles, a confident numerical prediction is rather sophisticated. An essential requirement is reliable experiments which may be used as a basis for model development and refinement and also for validating numerical calculations. However, at higher particle mass loading, e.g. in the range of 0.5–2 (the mass loading η is defined as the ratio of particle to gas phase mass flow rates), most of the phenomena described above are already strongly coupled. Hence, experiments for the independent analysis of the above-mentioned micro-processes are very difficult or even impossible.

A number of studies have been published in the past which are devoted to particle-laden pipe and channel flows with different boundary conditions. In one of the early investigations, the behaviour of rather large glass and copper beads in a long, narrow horizontal channel (channel length: 230 channel heights) made of glass was studied (Matsumoto and Saito 1970). The particle mass loading in these studies was kept mainly at around 0.5. However, the resulting relatively low number density (c_n, particles per unit volume) allowed the collision of particles with the walls to be analysed using cinematographic photography. This method also was the basis for the determination of the particles' angular velocity due to wall collisions. Even though rather large particles were considered, values of up to 2,000 r.p.s. were measured. Vertical profiles of the particle number density for different flow conditions showed a considerable increase towards the bottom of the channel which was associated with the action of gravity. The particle velocity was found to be almost constant across the channel.

In the studies of Burmester De Bessa Ribas et al. (1980), some experiments on a particle-laden flow in a rectangular horizontal channel were introduced for validating numerical predictions by a Monte Carlo kinetic model. The particles were glass beads with mean diameters of less than 0.5 mm. The particle mass loading was varied up to 3, and an average gas phase velocity in the range of 5–15 m/s was considered. The results demonstrate the effect of conveying velocity, particle size and mass loading on the established vertical profiles of solids concentration (c_n) and the effect of two-way coupling, namely the deformation of the profile of the horizontal gas velocity component. The main

emphasis in these studies, however, was related to the validation of the numerical model, which did not consider wall roughness, but inter-particle collisions.

A very detailed set of experiments was provided by Tsuji and Morikawa (1982) and Tsuji et al. (1984) for a gas–solid flow in narrow horizontal and vertical glass pipes. The test section length was 100 and 144 pipe diameters for the horizontal and vertical pipe, respectively. In both experiments, polystyrene spheres with a wide range of different mean diameters were used. The average gas velocity was varied in the range of 5 m/s to about 20 m/s, and the particle mass loading could exceed values of about 6. For the measurement of particle and gas velocity in the presence of the particles laser-Doppler anemometry was applied. The presented results focus on the two-way coupling effects in gas–solid flows. In both cases, the influence of particle size and mass loading on the streamwise mean velocity profiles of the gas phase was analysed. For the horizontal pipe a strong asymmetry was found for higher mass loading, i.e. above about 2, especially for the larger particles. Additionally, the papers provide detailed results on turbulence modulation. It was clearly demonstrated that large particles enhance turbulence considerably, whereas small particles damp turbulence. The data of Tsuji and Morikawa (1982) and Tsuji et al. (1984) were often used to characterise and parameterise turbulence modulation in gas–solid flows (Gore and Crowe 1989; Crowe 2000). In addition, Tsuji and Morikawa (1982) and Tsuji et al. (1984) presented turbulence spectra measured in the presence of the particle phase.

Kulick et al. (1994) experimentally analysed a downward directed gas–solid flow in a channel 40 mm high using a centreline gas velocity of about 10.5 m/s. The channel had a length of 130 channel heights, and a sophisticated feeding system was used, in order to ensure a homogeneous dispersion of the particles. The particles used in the experiment were Lycopodium particles and glass and copper beads with small diameters so that turbulence reduction was observed. Using these particles, a range of particle Stokes numbers, i.e. the ratio of particle response time to the turbulent time scale of the flow, $St=\tau_P/T_L$, could be considered. The main objective in this study was the analysis of turbulence modulation considering particle mass loading up to about 0.5. Unfortunately, the experiments were not done carefully enough with regard to wall boundary conditions, since the upper part of the test section consisted of coated wood plates, while a larger test section made of acrylic glass was used. Hence, the particle motion was far from being developed, as the wall collision properties completely change some distance above the measurement location. Since a channel flow is dominated by wall collisions (Sommerfeld 2000), a change in wall material can drastically affect the results, which was shown by several authors using, for example, large eddy simulations (e.g. Yamamoto et al. 2001). These simulations predict the correct behaviour in a downward flow, namely the particles move at a higher mean streamwise velocity than the gas flow. In the experiments on the other hand, the particle velocity was lower than the gas velocity (Kulick et al. 1994).

Recently, detailed studies on turbulence modification by particles in a vertical pipe were also performed by Varaksin et al. (1998, 1999). Unfortunately, a rather short test section of only 23 pipe diameters was used in the experiments. Small spherical glass beads were mainly used with a mass loading up to about 1. Based on the velocity measurements by laser-Doppler anemometry, a model was proposed, which describes all the data obtained on turbulence reduction by one non-dimensional parameter (Varaksin et al. 1998).

In order to provide experimental data for the validation of a Lagrangian wall collision model with wall roughness effects, Sommerfeld and Huber (1999) performed measurements in a narrow horizontal channel. A chopped Ar:ion laser was used to measure the change in particle velocity during a wall collision process based on the so-called streakline technique. Different wall materials were considered, such as stainless steel, polished steel, Plexiglas and rubber. The particles used were spherical glass beads with a diameter of 0.1 and 0.5 mm, respectively, and non-spherical quartz sand with a mean diameter of about 100 μm. The statistical averaged parameters for up to 5,000 single events allowed an improvement and detailed validation of the proposed stochastic wall collision model (Sommerfeld and Zivkovic 1992; Sommerfeld 1998; Huber and Sommerfeld 1998; Sommerfeld and Huber 1999).

Detailed experiments in different pipe elements 80 and 150 mm in diameter were performed using phase-Doppler anemometry (PDA) and a laser light sheet technique for particle concentration measurements by Huber and Sommerfeld (1994, 1998). The use of fine spherical seeding particles allowed measurement of gas and particle phase velocities simultaneously by the discrimination method proposed by Qiu et al. (1991). The particles were spherical glass beads with number mean diameters of 40 and 100 μm, respectively. A mass loading up to about 2 could be analysed in these studies. The experiments provided detailed information about the development of the cross-sectional particle concentration in different pipe elements. It was clearly demonstrated that wall roughness plays a significant role in the development of the particle concentration in different cross-sections of the pipe system by comparing results obtained with glass and stainless steel pipes. In horizontal pipes, the effect of gravitational settling is strongly reduced by wall roughness (Sommerfeld and Zivkovic 1992; Huber and Sommerfeld 1998). This is the result of the resuspension of the particles by wall roughness, caused by the fact that on average the rebound angle becomes larger than the impact angle for small particle trajectory angles, which are typical for pipe and channel flows (Sommerfeld and Huber 1999). As a consequence of the roughness, the wall collision frequency and the resulting pressure loss increased (Huber and Sommerfeld 1998). The latter is very important for the practical design of pneumatic conveying systems. Also, the numerical calculations with a simplified version of the wall collision model (Sommerfeld 1992), compared with that recently elaborated by Sommerfeld and Huber (1999), showed reasonable agreement with the experiments for particle concentration and velocity profiles in horizontal pipes.

However, a more generalised version of the wall collision model requires further experiments with different

levels of wall roughness. In addition, the other physical effects, such as inter-particle collisions and flow modulation, need to be carefully elucidated in order to interpret the experimental results. Therefore, a detailed experimental study on the particle behaviour in a particle-laden horizontal channel was performed. The horizontal channel was chosen, since gravitational settling causes an increase in particle concentration near the bottom. Hence, both wall roughness and inter-particle collisions will have a pronounced effect on the vertical profiles of particle concentration. In these studies, all relevant parameters were considered and varied, such as particle mass loading, particle size and average conveying velocity. For the first time, the importance of different degrees of wall roughness on the transport behaviour of the particle phase was analysed. It should be emphasised that the present experiments were only performed for spherical particles in the size range between 0.06 and 1.0 mm. Section 2 of the present paper contains a description of the experimental facility and Sect. 3 describes the applied optical instrumentation, namely PDA. The results of the measurements are presented in Sects. 4, 5 and 6, where the latter concentrates on the analysis of turbulence modulation.

2 Test facility

The entire test facility is shown in Fig. 1. The main component of the test facility was a horizontal channel 6 m long (about 170 channel heights), with a height H=35 mm and a width of 350 mm, so that almost two-dimensional flow conditions can be established in the core of the channel. This was validated by measuring vertical profiles of the air velocity at several lateral positions. For two air velocity profiles measured at ±60 mm lateral position from the core, the difference in the velocity values was less than 2%. The upper and lower channel walls were made of stainless steel plates which could be exchanged in order to study the effect of wall material and wall roughness on the particle behaviour. More information on the wall roughness structure will be provided below. The measurements were performed close to the end of the channel at a distance of 5.8 m from the entrance, to ensure almost fully developed flow conditions. In order to allow optical access for the phase-Doppler anemometer, the side walls were made of glass plates, and a glass window of 40 mm by 350 mm was inserted in the top wall. This window was mounted flush with the inner side of the wall plate to minimise disturbances. Also, the particle properties measured at this location will not be strongly affected, since particles are sampled which were rebound from the stainless steel walls at upstream locations. The numerical calculations of Sommerfeld (submitted, 2002) have shown that the mean free path between wall collisions λ_W is around 0.5–1.0 m, depending on particle size and degree of wall roughness.

The required air flow rate was provide by two roots blowers mounted in parallel with nominal flow rates of 1,002 m^3/h and 507 m^3/h, respectively. The blowers were connected with the test section using a 130-mm-pipe. Just before the channel, a mixing chamber for injecting the particles and a flow conditioning section were mounted, where the cross-section changes from circular to rectangular. Additionally, several sieves were inserted in this section in order to ensure homogeneous flow conditions at the entrance of the channel. In a straight section of 2 m before the mixing chamber, a flow meter and temperature, humidity and pressure sensors were installed. The flow rate was adjusted to be almost constant during each set of measurements with varying particle mass loading. The air temperature was on average around 30°C in all the measurements. In the results presented, three average air velocities U_{av} were considered. The characteristic properties of the single-phase channel flow are summarised in Table 1. The channel Reynolds number Re_H is defined as:

$$Re_H = \frac{\rho H U_{av}}{\mu}$$

For the determination of the Reynolds number, an air density of ρ=1.15 kg/m^3 and a dynamic viscosity of μ=18.62×10^{-6} N s/m^2 were used. The integral time scale of turbulence (T_L) on the centre of the channel was estimated from the following approximate relations for the turbulent kinetic energy k, and the dissipation rate ϵ in the following way (Milojevic 1990):

$$T_L = \frac{2}{9}\frac{k}{\varepsilon}$$

$$k = 0.5\left(u_{rms}^2 + 2v_{rms}^2\right)$$

$$\varepsilon = C_\mu^{0.75}\frac{k^{1.5}}{l_m}$$

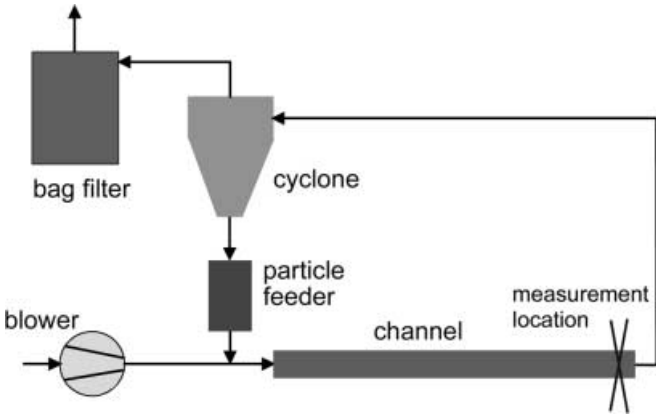

Fig. 1. Sketch of the horizontal channel test facility with the main components

Table 1. Characteristic properties of the single-phase channel flow for different Reynolds numbers

Average air velocity (m/s)	Channel Reynolds number	Integral time scale on centreline (ms)	Kolmogorov time scale, centreline (ms)
14.25	30,805	5.0	0.87
19.7	42,585	3.7	0.54
26.5	57,284	3.1	0.41

Here, the fluctuating velocities of air in the streamwise and transverse direction, u_{rms} and v_{rms}, were obtained from the measurements on the centreline and the dissipation rate was estimated with C_μ=0.09 and a mixing length of l_m/H=0.07 (Schlichting 1965). The Kolmogorov time scale τ_K was calculated according to:

$$\tau_K = \left(\frac{\nu}{\varepsilon}\right)^{1/2}$$

where ν is the kinematic viscosity of air.

For feeding the particle material into the mixing chamber, a screw feeder (K-TRON, Type K2MV S60) was used, whereby the particle mass flow rate could be adjusted accordingly. In order to ensure continuous particle feeding, the air was injected into the mixing chamber through a converging nozzle, whereby a lower pressure and a high velocity were established. The resulting jet entered the exit pipe of the mixing chamber on the opposite side. This procedure also ensured a good dispersion of particles and tracer, and possible agglomerates were destroyed.

A 90° bend was mounted at the end of the channel. It was connected to a flow passage where the cross-section changes from rectangular to circular. A flexible pipe was used for conveying the gas–particle mixture to a cyclone separator. The separated particles were reinjected into the reservoir of the particle feeder through a bucket wheel. Finally, the air from the cyclone passed through a bag-filter with pulse-jet cleaning, in order to remove very fine particles (mainly the tracer particles) and was released into the environment.

The particles used in the experiment were spherical glass beads with different mean diameters D_p and size distribution as summarised in Table 2. The size distributions were obtained by using a phase-Doppler anemometer with an optical configuration described below. It should be mentioned that in addition 1-mm glass beads were used. However, owing to the limited sizing range of the phase-Doppler anemometer, only the air velocity was measured in this case. Moreover, it should be mentioned that rather large particles were used so that adhesion forces were not of great importance and the particles could be easily dispersed. Also, in the considered range of air velocities, no sticking of the particles on the walls or formation of ropes on the bottom wall of the channel could be observed. Such phenomena are only observed at lower air velocity.

For providing an impression about the particles response characteristics to the turbulent fluctuations of the air phase, particle Stokes numbers are also given in Table 2 for the flow with Re_H=42,585. The particle response time τ_p was calculated by:

$$\tau_p = \frac{\rho_p D_p^2}{18\mu f_d}$$

where ρ_p is the particle material density, D_p the particle diameter and $f_d = 1.0 + 0.15Re_p^{0.687}$ is the non-linear term of the particle drag coefficient, which was calculated in an iterative way by using the terminal velocity of the particles $U_{p,\infty}$ in the particle Reynolds number:

$$Re_p = \frac{\rho D_p U_{p,\infty}}{\mu}$$

As the characteristic time scale of turbulence, the integral time scale T_L on the centre of the channel for single-phase flow was selected as described above. The results in Table 2 show that the Stokes number for the smallest particles (60 μm) is 5.01, indicating that their motion is not very strongly affected by turbulence. For the 625-μm particles, the Stokes number is about 386, hence they will be not influenced by turbulence. During the experiments, no considerable degradation or erosion of the particles was observed, so that resulting errors in the PDA measurement could be excluded. Nevertheless, the particle material was frequently renewed.

For the experiments, stainless steel walls (upper and lower wall along the entire channel) with two degrees of wall roughness were used, namely plates with low (R1) and high (R2) degree of roughness. Typical roughness profiles are shown in Fig. 2, obtained by a Paertometer (Type S3P) which mechanically scans the surface. By numerically scanning this roughness profile with different sampling distance, one can obtain the degree of roughness experienced by different sized particles, as demonstrated by Sommerfeld and Huber (1999). The relevant roughness dimension is the average value of the difference between neighbouring maxima and minima of the roughness structure. These values are summarised in Table 3 for the streamwise and lateral directions (R_x and R_y), together with the respective maximum values ($R_{x,max}$ and $R_{y,max}$).

With the test facility described above, average air velocities up to 30 m/s and a particle mass loading up to about 2 could be established. However, it should be noted that, for smaller particles, a higher loading could not be considered due to the resulting high particle number density c_n and the limits for the application of optical measurement techniques. In order to maintain a constant air flow rate with variation in mass loading, the air flow rate

Table 2. Characteristic diameters and properties of the different spherical glass beads (material density ρ_p=2500 kg/m^3) used in the experiment (the particle Stokes number was calculated based on the integral time scale on the centreline of the channel for an average air velocity of 19.7 m/s)

Particle nominal size (μm)	Particle size range (μm)	Number mean diameter (μm)	Standard deviation (μm)	Sample size range for velocity measurements (μm)	Particle response time (ms)	Particle Stokes number
60	25–75	52	9.6	45–65	18.3	5.01
100	70–130	100	14.5	90–110	63.0	17.2
190	130–230	190	21.5	180–210	189.0	51.7
625	470–800	625	59.0	530–700	1410.0	386.0

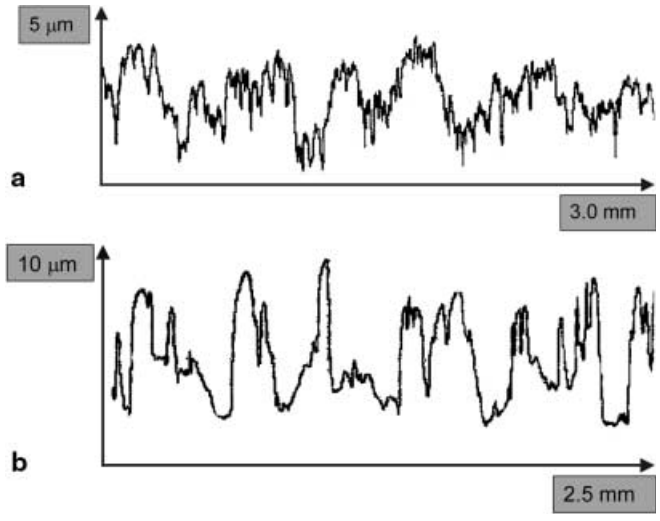

Fig. 2a, b. Measured profiles of surface roughness for a stainless steel plate: **a** low degree of roughness (R1); **b** high degree of roughness (R2) (both axes are linear, and the values specified on the axis indicate exactly the entire length of the horizontal and vertical axis)

was readjusted for each experiment. The maximum variation in the air flow rate for one series of measurements with constant air velocity and varying particle mass loading was about 2.5%. The air temperature at the channel entrance varied between about 25 and 35°C, depending on the environmental temperature. For an almost constant ambient pressure, this resulted in an air density variation of about ±1.7% around a mean value of 1.15 kg/m^3. The particle flow rate from the screw feeder was subject to some fluctuations due to the feeding screw, but became almost constant as a result of the mixing chamber design. The repeatability of the measurements was in the range as expected from variations in temperature and air flow rate.

3 Instrumentation

For the simultaneous measurement of both, particle phase and continuous phase properties, PDA was applied. The PDA technique allowed the time-averaged velocities of both phases to be determined with a good spatial resolution, and additionally, the local particle size distribution. In order to allow for a measurement of the continuous phase velocities in the presence of the particles, spherical seeding particles (Ballotini 10002A) were added to the flow with a nominal size of about 4 μm. This was accomplished by mixing the tracer particles with the dispersed phase particles in the reservoir of the particle feeder. The discrimination procedure was based on size measurement according to Qiu et al. (1991) and will be described in more detail below.

The transmitting and receiving optics of the two-component PDA (Dantec Fiber PDA) were mounted on a common, computer-controlled traversing system as illustrated in Fig. 3. In order to ensure high scattering intensities for the tracer particles, the receiver was mounted at a scattering angle of 33.5°. At this angle, a fairly linear phase–size relation is established, as demonstrated by Sommerfeld and Tropea (1999) using Mie calculations. Vertical profiles of the properties of both phases were measured close to the end of the channel (5.8 m from the entrance) in the middle plane. The measurement of the horizontal and vertical components of the velocities of both phases up to the lower and upper channel walls was only possible, however, by tilting the entire traversing system. Therefore, both sides of a horizontal traversing bar carrying the transmitting and receiving fibre probes could be moved independently. Measurements near the upper wall were performed by turning the traversing system in such a way that the upper beam for measuring the vertical velocity component was parallel to the channel wall. Near the centre of the channel, the traversing system was tilted by computer control, so that the lower beam was parallel to the lower wall (Fig. 3). Hence, completely computer-controlled measurements were possible across the channel height.

The optical configuration of the PDA system was selected according to the particle sizes considered. For the different experiments, a 500-mm transmitting lens and a 400-mm receiving lens were used. The sizing range could be changed by inserting different masks in the receiver, whereby the elevation angle of the three detectors could be varied. For glass beads with a refractive index of 1.51, a sizing range of 266 μm was possible with mask A and 1,032 μm with mask C. The optical parameters of the PDA system are summarised in Table 4 for both components.

A typical measurement of the combined size distribution of tracer particles and dispersed phase particles is shown in Fig. 4 together with the size–velocity correlation for three locations in the channel, i.e. in the centre of the channel and 0.03 and 0.29 channel heights from the bottom wall. The vertical axis indicates the number of validated samples for the different size classes. At each measurement point, a sufficiently large number of samples (minimum 8,000 samples for each phase; see Fig. 4) were collected, in order to allow for statistically reliable measurements (small confidence levels of mean and rms values) of the mean and fluctuating velocity components of both phases. From Fig. 4, it is obvious that a clear separation of the size distributions of tracer and dispersed phase particles is possible. The comparison of the number of samples for the tracer particles collected at different locations shows a decrease when the optical path length for the receiving optics increases in the two-phase flow and

Table 3. Wall roughness characteristics of the two different stainless steel walls used in the experiments (R_x, R_y mean values; $R_{x,max}$, $R_{y,max}$ maximum values)

Degree of wall roughness	Streamwise direction (x)		Transverse direction (y)	
	R_x (μm)	$R_{x,max}$ (μm)	R_y (μm)	$R_{y,max}$ (μm)
Low roughness R1	4.26	6.94	3.47	4.04
High roughness R2	6.83	8.32	6.89	7.83

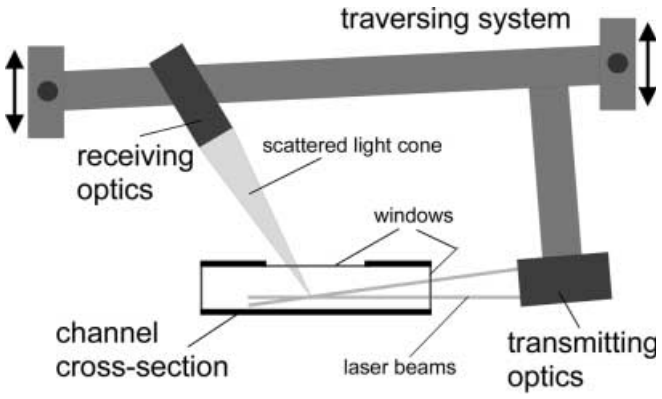

Fig. 3. Installation of the PDA on the computer-controlled traversing system

Table 4. Optical parameters of the PDA system

Transmitting lens	500 mm
Receiving lens	400 mm
Beam separation	35 mm
Wavelength of green laser beam	514.5 nm
Wavelength of blue laser beam	488 nm
Gaussian beam diameter	1.35 mm
Fringe spacing of green laser beam	7.35 μm
Fringe spacing of blue laser beam	6.97 μm
Probe volume length of green laser beam	6.936 mm
Probe volume length of blue laser beam	6.579 mm
Probe volume diameter of green laser beam	0.243 mm
Probe volume diameter of blue laser beam	0.230 mm
Velocity range green (*u*-component)	±44.1 m/s
Velocity range blue (*u*-component)	±4.19 m/s
Scattering angle	33.5°
Particle refractive index	1.51
Sizing range mask A	266 μm

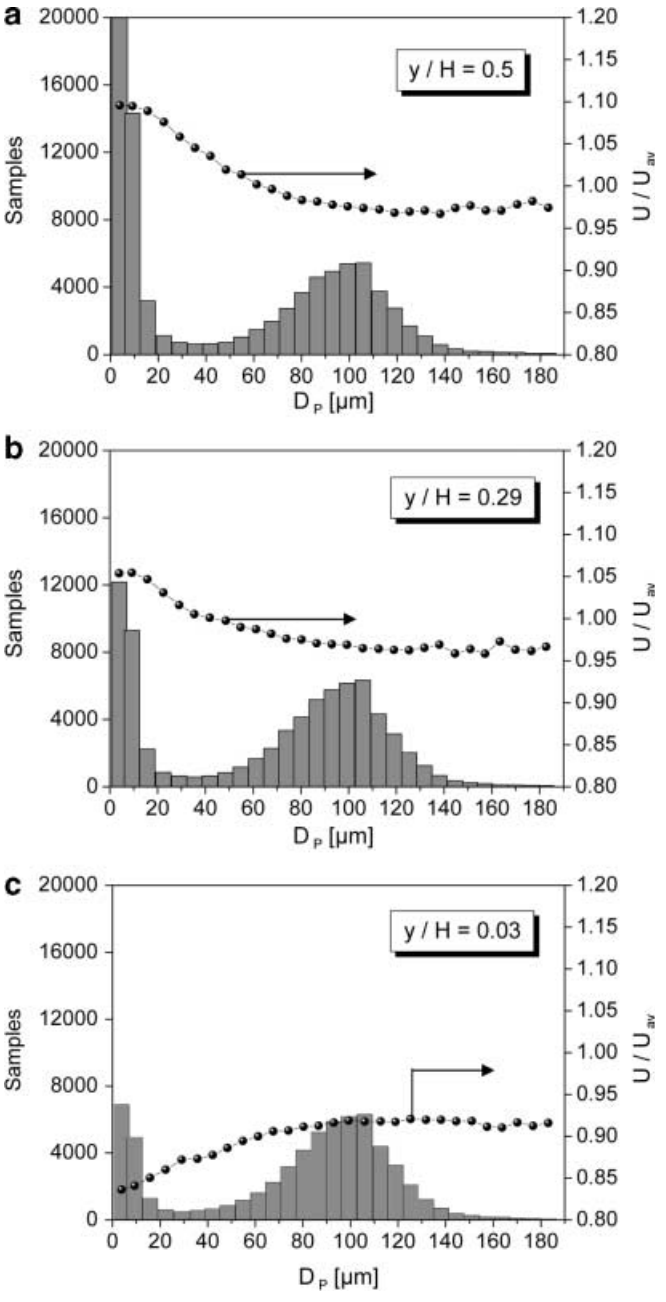

Fig. 4a–c. Size distribution of tracer and dispersed phase particles (*vertical bars*) together with the size velocity correlation (*lines with symbols*): **a** y/H=0.5, centre of the channel; **b** y/H=0.29; **c** y/H=0.03 (U_{av}=19.7 m/s; 100-μm glass beads; η=0.3; low roughness R1; y distance from lower wall)

the measurement location moves towards the bottom of the channel (see Fig. 3). This shows the effect of light absorption by the dispersed phase particles, which causes a decrease in the data rate for the tracer. The velocity information for the air phase was obtained from particles smaller than 7 μm. The size–velocity correlation shows that, in the first two size classes, the axial velocity component is almost constant and hence, represents the air velocity correctly. Even in the vicinity of the wall with small turbulent time scales and large velocity gradients, the variation in the tracer velocity in the size range up to 7 μm was found to be less than 1% (Fig. 4c). Also, the mean and fluctuating velocities of the particles were not determined over the entire size range, but only in a certain range around the maximum of the respective size distribution. In Table 2, the sample size range for the different particles used in the experiment is summarised.

Since the commercial PDA-software did not allow for accurate determination of particle concentration, the raw data were reprocessed after the measurements in order to allow a better estimation of this value across the channel. Essential for concentration measurements is the estimation of the probe volume cross-section as a function of the direction of particle motion (Sommerfeld and Qiu 1995). As the particle motion may be considered to be essentially two-dimensional in the channel flow considered, and a two-component PDA system was used, the cross-section of the probe volume perpendicular to the particle motion is determined from (Zhang and Ziada 2000):

$$A_{p\perp} = \frac{\pi}{4} d_e^2 \frac{1}{\tan\varphi} \left| \frac{v_p}{\mathbf{u_p}} \right| + d_e L$$

where d_e is the diameter of the probe volume given by the e^{-1} value of the light intensity distribution, φ is the off-axis

angle of the receiver, L is the length of the probe volume imaged onto the receiving optics, v_p is the instantaneous transverse particle velocity component (perpendicular to the main stream component), and $\mathbf{u}_p$ is the absolute value of the two relevant particle velocity components (streamwise and transverse component). Since rather large and almost monodisperse particles are considered, the variation in the probe volume cross-section with particle size was not accounted for. Hence, the number concentration of the particles c_n was calculated with the number of samples (N_p) and the total measurement time (T_{samp}) in the following way:

$$c_n = \frac{N_p}{\frac{1}{N_p}\sum_{i=1}^{N_p}\left(A_{p\perp}\sqrt{u_p^2+v_p^2}\right)T_{samp}}$$

Here u_p and v_p are the components of the instantaneous particle velocity in the streamwise and transverse direction, respectively. Since rejected Doppler signals were ignored in this evaluation, the absolute values of the measured particle concentration are not very reliable. Therefore, the results on particle number concentration c_n are presented as normalised values, i.e. the measured number concentration is always divided by the measured average value obtained across the channel $c_{n,av}$.

4
Single-phase flow

In order to prove the quality of the established channel flow, air-phase measurements were compared with data from the literature. Similar to Kulick et al. (1994), the present velocity measurements were compared with the experiments of Hussain and Reynolds (1975) and the large-eddy simulations (LES) of Moin and Kim (1982) as shown in Fig. 5. The LES data were chosen, since the channel Reynolds number was in the range of the present experiments, namely about 25,000. The mean streamwise component of the air velocity is normalised by the friction velocity U_z which is obtained from (Hussain and Reynolds 1975):

$$\frac{U_\tau}{U_0} = 0.1079 Re_h^{-0.089}$$

Here U_0 is the centreline mean velocity and the channel Reynolds number Re_h is obtained with the half channel height h=H/2 in this case. The normalised wall coordinate is given by:

$$y^+ = \frac{yU_\tau}{\nu}$$

For clarity, the streamwise rms velocity fluctuation u_{rms} is normalised by the centreline air velocity U_0, and the wall distance y by the half channel height h. The profile of the streamwise mean velocity agrees well with the previous measurements (Hussain and Reynolds 1975) and the LES (Moin and Kim 1982). It should be noted that the present measurements were not performed to resolve the particle behaviour in the vicinity of the walls. Therefore, the fluid and also the particle velocity were obtained up to a location of about 1 mm from the wall. In Fig. 5b, the measured streamwise rms velocity fluctuation is compared with the literature data. The agreement is reasonably good, especially for normalised wall distances smaller than about 0.6. The larger mean fluctuating velocities in the core of the channel (about 30% larger than the LES and 13% larger than the experiments) are presumed to be caused by the higher wall roughness considered in the present studies. These measurements were performed with the higher roughness R2.

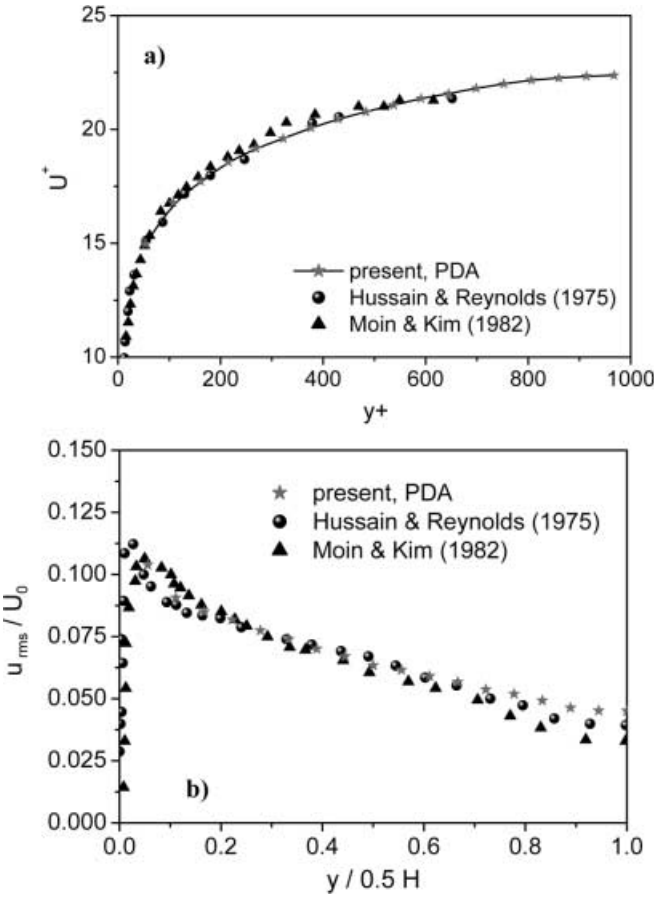

Fig. 5a, b. Comparison of single-phase velocity measurements with literature data obtained from measurements (Hussain and Reynolds 1975) and LES (Moin and Kim 1982): **a** normalised streamwise mean velocity; **b** normalised streamwise rms velocity fluctuation (average gas velocity on centreline U_0 = 21.77 m/s; high roughness R2)

5
Two-phase results

Two-phase flow experiments were performed in order to analyse the influence of the following parameters on the particle phase properties (mean velocity, fluctuating velocities and concentration) and the modulation of the air flow (air mean velocities and turbulence):

- Particle mass loading;
- Particle size and size distribution;
- Air flow rate, i.e. conveying velocity;
- The degree of wall roughness and wall material.

In all the profiles presented, the streamwise and lateral mean velocities (U, V and U_p, V_p) and the associated

fluctuating components (u_{rms}, v_{rms} and $u_{p,rms}$, $v_{p,\,rms}$) for both phases are normalised by the average single-phase air velocity U_{av}. The particle number density c_n is normalised by the average number density $c_{n,av}$ for the considered mass loading. It should be noted that all cases with different mass loading η, specified in the legend, are not shown in the graphs for clarity. A typical set of measurements for the 100-μm particles and the low roughness wall (R1), illustrating the effect of mass loading, is shown in Fig. 6. This is a case where a relatively strong turbulence attenuation is observed. The profiles of the air and particle velocity in the horizontal direction (U and U_p) indicate that the particles are slower than the air phase in the core region, which is the result of particle inertia. The transverse dispersion of the particles and their slip boundary condition at the walls give velocities higher than that of the air phase in the near-wall region. Hence, for such a condition, the slip-shear lift force will act towards the wall in the near-wall region and towards the centre in the core of the channel (Sommerfeld 1996). With increasing mass loading η, the air velocity profile is flattened as a results of the increased coupling between the phases. The reduction in the air velocity in the core of the channel is found for all cases. However, for the low wall roughness condition, the air velocity increases near the bottom and, hence, the profile becomes asymmetric with increasing mass loading. This is associated with the higher particle number concentration c_n near the bottom (see Fig. 9b). The streamwise particle velocity profiles (Fig. 6a) exhibit a slight increase in the average particle velocity U_p with an increase in mass loading. This is caused by the enhancement of transverse particle dispersion through inter-particle collisions and a reduction in the wall collision frequency resulting from this phenomenon, as will be shown below (submitted, Sommerfeld, 2002).

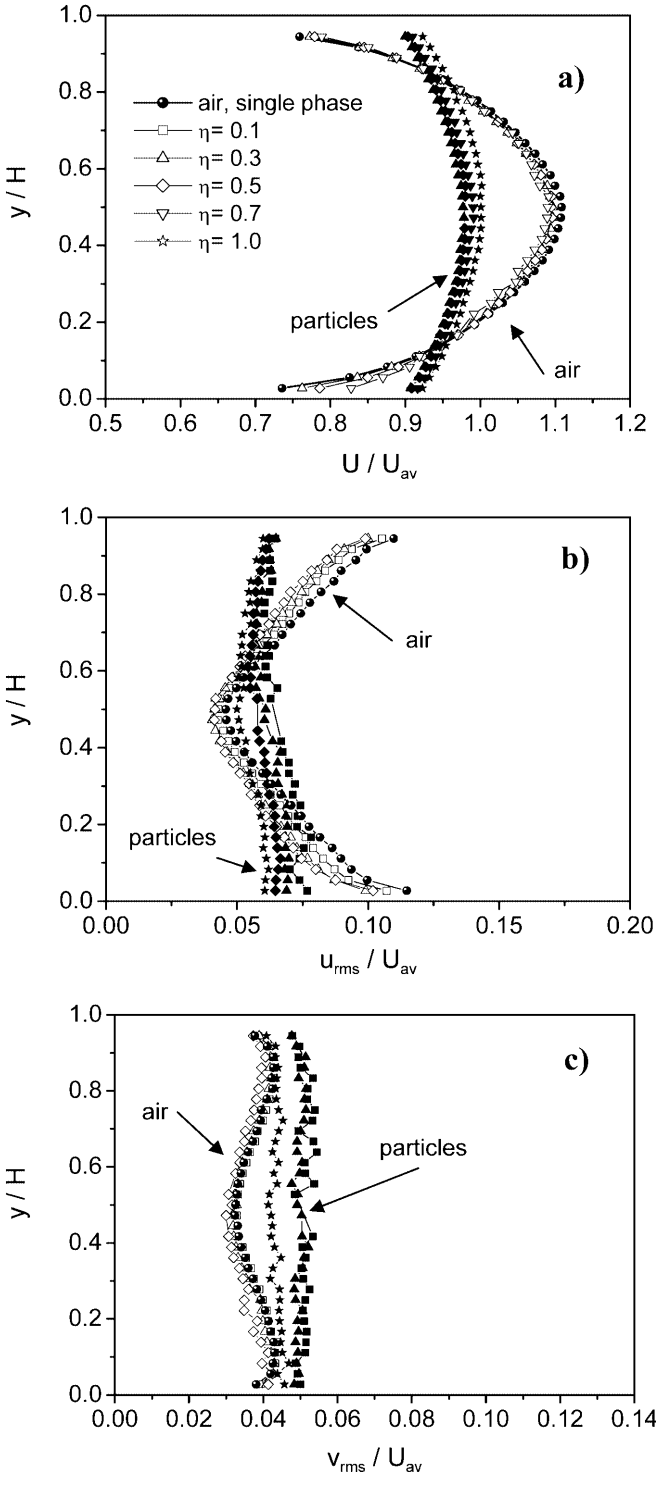

Fig. 6a–c. Vertical profiles for air and 100-μm particles with U_{av}=19.7 m/s for the low roughness case (R1): **a** horizontal mean velocities of air and particles; **b** horizontal component of rms velocity fluctuation; **c** vertical component of rms velocity fluctuation (*open symbols*: air; *closed symbols*: particles)

The profiles of fluctuating velocities of the air phase (u_{rms} and v_{rms}) corroborate the effect of turbulence attenuation for such small particles. However, it should be noticed that this effect is much more pronounced for the horizontal component than for the vertical one.

The fluctuating velocities of the particles are considerably damped for both components ($u_{p,rms}$ and $v_{p,rms}$) with increasing loading. Since rather inertial particles are considered, this is only marginally caused by the damping of fluid turbulence. The damping of particle fluctuation is mainly caused by inelastic inter-particle collisions, whereby energy is dissipated in the deformation process.

In the corresponding case with the high wall roughness (R2), similar effects are observed for the profiles of the horizontal velocity components (Fig. 7). However, due to the increase in wall collision frequency associated with the roughness, considerable lower particle mean velocities U_p are observed compared with the low roughness, which is a consequence of the average increase in momentum loss for the particle phase. Moreover, both components of the particle mean fluctuating velocity ($u_{p,rms}$ and $v_{p,rms}$) are considerably enhanced by the irregular wall-bouncing process compared with the low roughness case (Fig. 6). In addition, a stronger reduction in the fluctuation intensity of particles ($u_{p,rms}$ and $v_{p,rms}$) with particle loading is observed here. This is caused mainly by the increasing inter-particle collision frequency. Additionally, the fluctuating motion of the particles becomes more isotropic as a consequence of wall roughness. The attenuation of flow turbulence with increasing loading η is slightly stronger for the higher wall roughness, which is a result of the increased slip velocity and the enhanced particle fluctuating motion.

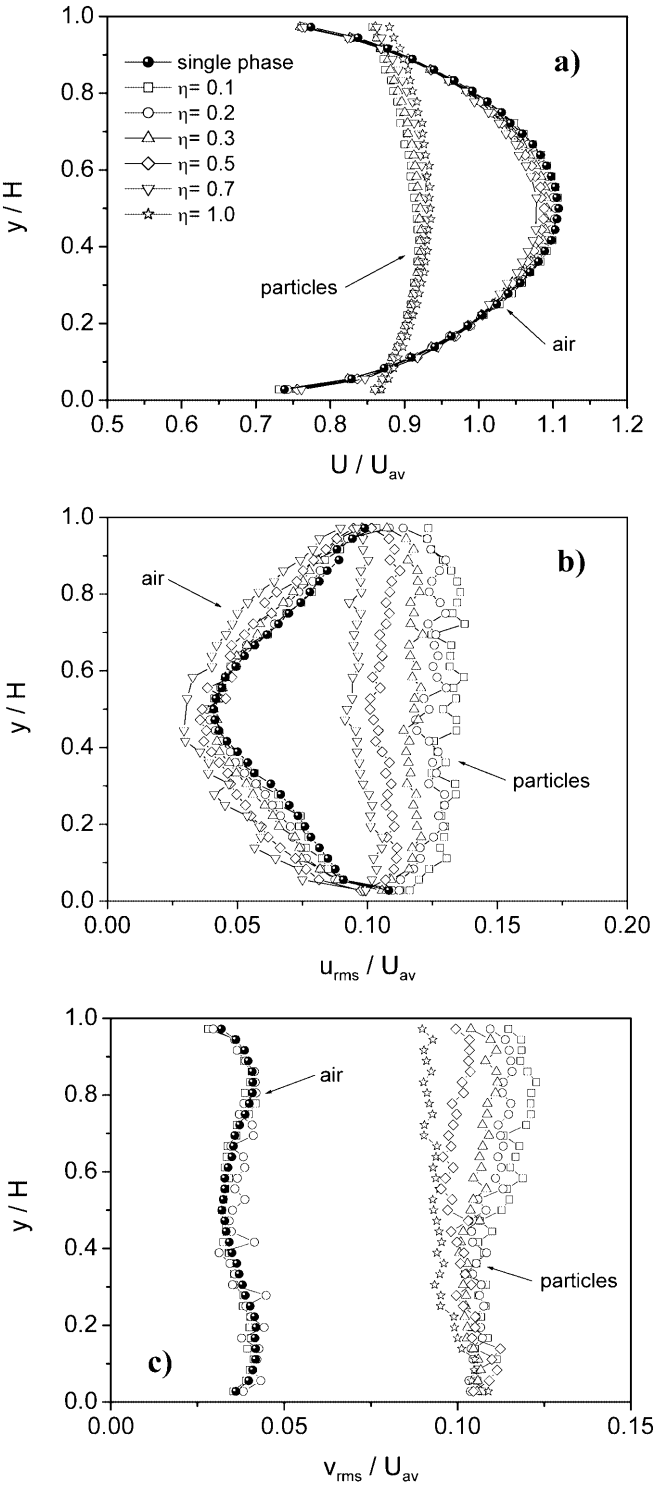

Fig. 7a–c. Vertical profiles for air and 100-μm particles with U_{av}=19.7 m/s for the high roughness case (R2): **a** horizontal mean velocities of gas and particles; **b** horizontal component of rms velocity fluctuation; **c** vertical component of rms velocity fluctuation

A quite interesting phenomenon is observed in the vertical component of the mean particle velocity V_p (Fig. 8). For a fully developed flow, this velocity component should be close to zero across the channel. This was also confirmed for the measurements with low roughness walls. In the case of the higher wall roughness however, the transverse

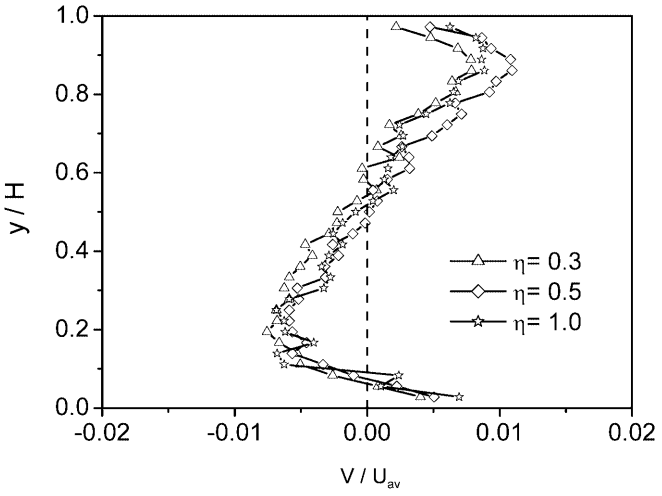

Fig. 8. Profiles of the vertical component of the particle mean velocity (average conveying velocity U_{av}=19.7 m/s; high roughness case (R2); 100-μm particles)

component of the particle mean velocity shows a Z-shaped profile. Obviously, this is a result of wall roughness and may be explained as follows. For a smooth wall, the velocities of particles being rebound from the wall is slightly lower than the impact velocity due to dissipation effects. For a rough wall, on the other hand, the so-called shadow effect becomes of importance, which is associated with the fact that the probability is larger for a particle to hit an ascending, rather than a falling part of the roughness structure. This effect implies that the wall-normal velocity component of the particles after rebound is on average larger than the corresponding impact velocity for small impact angles up to about 10–15° (Sommerfeld and Huber 1999). Hence, the transverse particle velocity V_p is shifted towards positive values very near the bottom of the channel, as illustrated in Fig. 8. Accordingly, a negative normal velocity should be found close to the top wall, which is probably not resolved by the measurements. As a result, the combined velocity PDF of impinging and rebounding particles for the wall-normal component is shifted towards positive values in the lower half of the channel, and negative values of this velocity component should prevail near the upper wall. However, a clear bimodal distribution of the normal velocity component near the walls could not be found, mainly due to the irregular rebound of the particles, which was shown by Sommerfeld and Kussin (submitted, 2002) in comparing measurement and calculation. In the regions between $0.1<y/H<0.5$ and $0.5<y/H<0.9$, the particles are on average moving towards the wall. This observation implies that the gas–particle flow seems to be not yet fully developed for higher wall roughness. Numerical calculations by Sommerfeld and Kussin (submitted, 2002) revealed that even a channel 12 m long, i.e. about 343 channel heights, was not sufficient to obtain zero transverse particle velocity V_p across the channel. However, due to the small velocities involved, a strong change of the particle concentration profile between 6 and 12 m could not be observed, i.e. less than about 5%.

The particle concentration profiles also exhibit the characteristic features of a gas–solid flow in horizontal

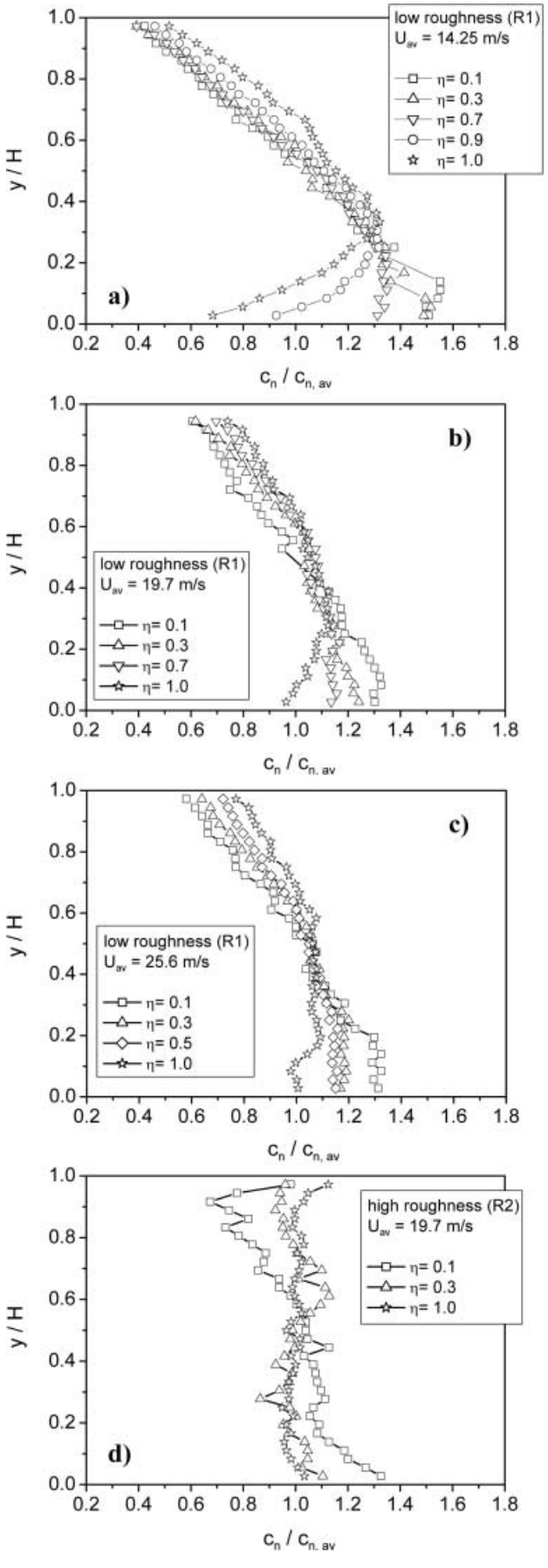

◀

Fig. 9a–d. Vertical profiles of normalised particle concentration profiles for different conditions in the case of 100-μm glass beads: **a** low roughness (R1), U_{av}=14.25 m/s; **b** low roughness (R1), U_{av}=19.7 m/s; **c** low roughness (R1), U_{av}=25.6 m/s; **d** high roughness (R2), U_{av}=19.7 m/s

channels and demonstrate clearly the effects of inter-particle collisions. The results shown in Fig. 9 demonstrate the influence of mass loading, average conveying velocity and the degree of roughness. In the case of low roughness, the trends are very similar. At low mass loading η, an almost linear increase in the solids concentration c_n from the upper to the lower wall is observed. This implies that a saltatory motion of the particles along the bottom wall of the channel is dominant, which is only partly balanced by turbulent dispersion effects. With increasing mass loading, inter-particle collisions in the region of high particle concentration near the bottom wall increasingly influence the particle behaviour. This results in a re-dispersion of the particles in the channel, i.e. particles from the high concentration region near the bottom are ejected due to inter-particle collisions, as demonstrated by Sommerfeld (submitted, 2002) using numerical calculations. Eventually, at higher particle mass loading η, the increasing collision frequency results in a shift in the concentration maximum towards the centre of the channel.

This phenomenon may be explained as follows. Particles approaching the wall will preferably collide with particles coming from the wall after reflection and thereby rebound towards the core region of the channel. This effect results in a reduction in the particle concentration, especially near the bottom wall, and the concentration maximum is continuously shifted to some distance above the bottom with increasing mass loading. In the case of lower roughness, this phenomenon is most pronounced for the smaller conveying velocity U_{av} (Fig. 9a), since the role of turbulence and wall roughness become less important and inter-particle collisions play the dominant role. The resulting parabolic shape of the concentration profile at high mass loading and for U_{av} = 14.25 m/s could also be identified as being caused by inter-particle collisions using Lagrangian numerical calculations (submitted, Sommerfeld and Kussin, 2002). With increasing conveying velocity U_{av}, the lateral particle dispersion increases, mainly due to wall collisions and roughness, but also due to the increasing importance of turbulence. However, the difference for the conveying velocity of 19.7 m/s and 23.7 m/s (Fig. 9b, c) is very small, indicating some kind of saturation in the dispersion process. For conditions of high wall roughness (Fig. 9d), the collision of particles with the walls predominates. Hence, almost constant particle concentration profiles are established even at low mass loading η. The slight increase in the particle concentration c_n towards the wall is presumed to be the result of the slip-shear lift force which is acting towards the wall in this region.

For the 190-μm particles and the rough wall (R2) the conveying behaviour is quite similar to that described above for the 100-μm particles, which results in the same trends for the particle concentration profiles. The essential

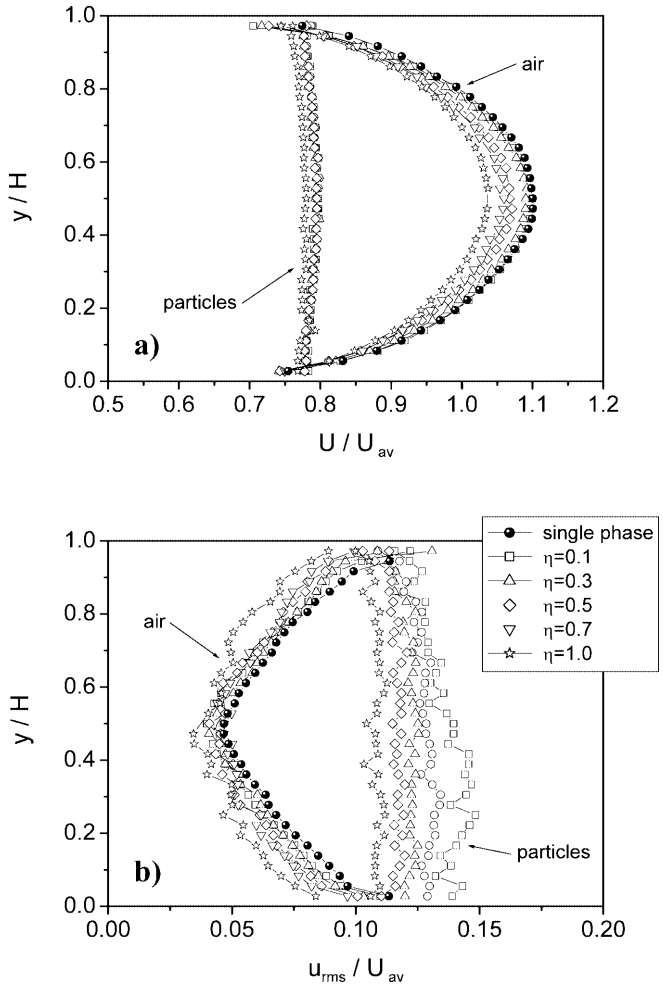

Fig. 10a, b. Vertical profiles for air and 190-μm particles with U_{av}=19.7 m/s for the high roughness case (R2): **a** horizontal mean velocities of gas and particles; **b** horizontal component of rms velocity fluctuation

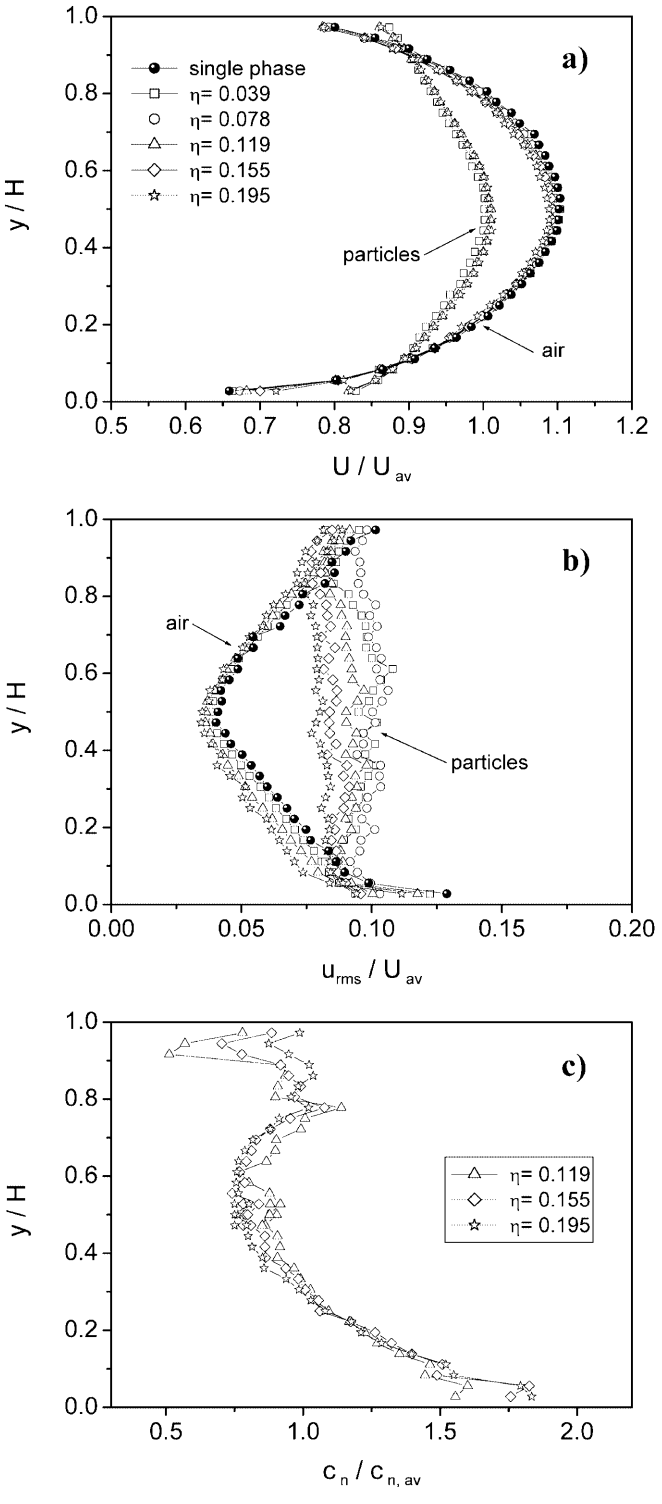

Fig. 11a–c. Vertical profiles for air and 60-μm particles with U_{av}=19.7 m/s for the high roughness case (R2): **a** horizontal mean velocities of gas and particles; **b** horizontal component of rms velocity fluctuation; **c** normalised particle number concentration

difference however, is larger particle inertia and, hence, the resulting larger slip velocity (Fig. 10). This also results in a stronger momentum coupling with the air phase, and an increasing particle mass loading η gives a larger reduction in the streamwise air velocity U in the core of the channel. In addition, it may be observed that the profiles for the horizontal component of the particle velocity U_p become flatter compared with the 100-μm particles. This is a result of the more pronounced influence of wall collisions and the associated slightly higher velocity fluctuation of the particles (compare Fig. 7b and Fig. 10b). The reduction in the streamwise component of the air phase fluctuation u_{rms} (turbulence modulation) with increasing particle mass loading is similar for the 100- and 190-μm particles.

In contrast, the smallest particles considered in the experiment (nominal diameter of 60 μm), transported in the channel with the rough walls, show a considerable lower slip velocity and therefore also a smaller modulation of the mean streamwise air velocity profile (Fig. 11). Both the air and particle mean velocity profiles (U and U_p) are non-symmetric in this case. This is caused mainly by the higher particle concentration c_n in the lower half of the channel (Fig. 11c) and the associated higher wall collision frequency of the particles with the bottom wall. This eventually reduces the particle and air velocities. The horizontal component of the particle rms velocity fluctuation ($u_{p,rms}$) is considerably lower than for the other two cases. It is obvious, however, that the decrease with

increasing mass loading becomes stronger due to the increased inter-particle collision frequency, which is a consequence of the higher number density c_n for the same mass loading. Moreover, the reduction in the air phase turbulence by the particles is concentrated in the lower half of the channel. This phenomenon is also supported by the profiles of the particle concentration c_n for these cases. Since the particles respond more easily to air flow and turbulence, their motion is less dominated by wall collisions. However, turbulence is not sufficient to completely disperse the particles and, therefore, gravitational settling results in a considerably higher solids concentration near the bottom of the channel. Increasing mass loading η in the considered range, and hence inter-particle collision frequency, results in only a slight modification of the normalised concentration profiles.

In order to further assess the influence of the different parameters on the particle behaviour in the horizontal channel, the results for the particle diameters considered, particle mass loading and the two degrees of roughness are directly compared. The profiles of the particle mean velocities U_p in comparison with the single-phase air velocity U of course show that an increase in particle size results in a decrease in particle velocity U_p and hence, an increase in slip velocity in the core of the channel (Fig. 12). In the near-wall regions, the particles are faster than the air flow due to the transverse dispersion and the slip boundary condition. The extent of this region decreases with increasing particle diameter. Obviously, an increasing particle size diminishes the response of the particles to the air flow, and the transverse dispersion due to wall collisions is enhanced, whereby the streamwise particle velocity profiles become more flattened. The increase in wall roughness causes, in the particle size range considered, an enhancement of transverse dispersion and, hence, an increase in wall collision frequency (or reduction in the wall collision mean free path). This, on the other hand, enlarges the momentum loss in the wall bouncing process and therefore, a remarkable decrease in particle mean velocity U_p is observed due to the wall roughness (Fig. 12).

The vertical profiles of the streamwise particle rms velocity fluctuation ($u_{p,rms}$) for different particle sizes demonstrate again the enhancement of the fluctuating motion with increasing particle size, which is a consequence of particle inertia and wall collision behaviour (Fig. 13). For increasing particle diameter, their motion becomes increasingly wall-collision dominated, whereby they bounce from wall to wall. However, it is clearly observed that the fluctuating velocities approach some limiting value with increasing particle diameter.

In order to compare the different experimental conditions directly, the normalised particle fluctuation energy E_p is calculated according to:

$$E_p = \frac{u_{p,rms}^2 + v_{p,rms}^2}{U_{av}^2}$$

and averaged across the channel to yield $E_{p,av}$. Here $u_{p,rms}$ and $v_{p,rms}$ are the local streamwise and lateral mean fluctuating velocities of the particle phase. From the results shown in Fig. 14, the following conclusions may be drawn:

- The increase in the wall roughness results in a drastic enhancement of the normalised particle fluctuating energy $E_{p,av}$.
- With increasing particle mass loading, $E_{p,av}$ is reduced for a given particle size, mainly due to the energy dissipation involved in the inter-particle collision process.
- In the particle size range considered, the fluctuating energy $E_{p,av}$ increases with diameter due to particle inertia and wall bouncing, i.e. wall-collision dominated behaviour of large particles.
- The rate at which the particle fluctuating energy decreases with mass loading η is more pronounced for a higher wall roughness and increases with decreasing particle size.

The latter is mainly provoked by inter-particle collisions, which become more important for higher fluctuation values (e.g. due to wall roughness). Moreover, a reduced particle size implies an increased particle number

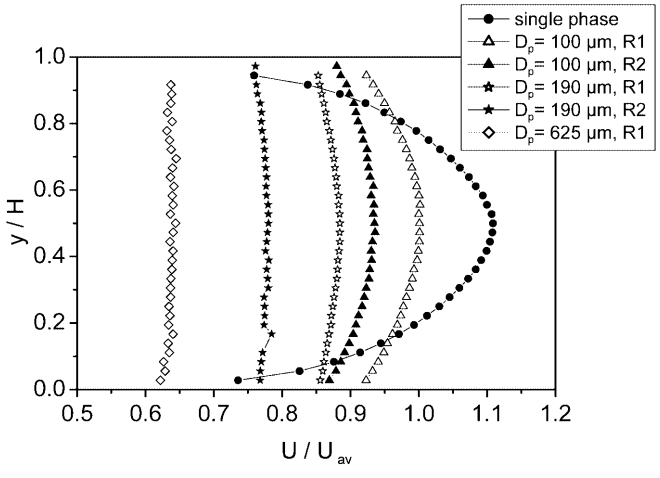

Fig. 12. Vertical profiles of the streamwise velocity component for different particle diameters and the cases with low (R1) and high (R2) roughness (U_{av}=19.7 m/s; η=1.0)

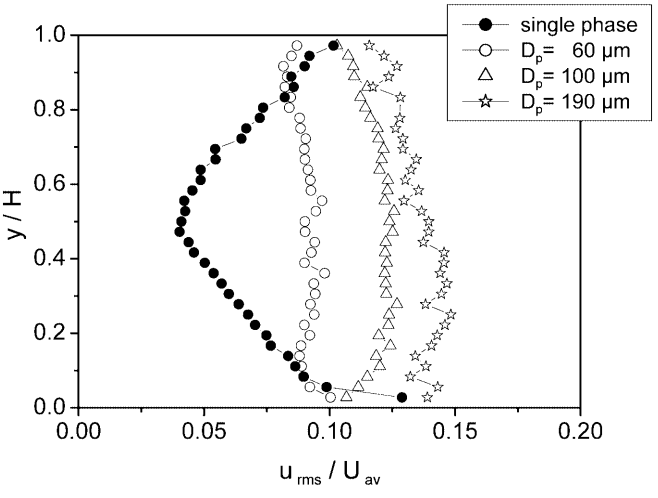

Fig. 13. Profiles for the horizontal component of rms velocity fluctuation comparing different particle diameters for the case of high roughness R2 (U_{av}=19.7 m/s; η=0.5)

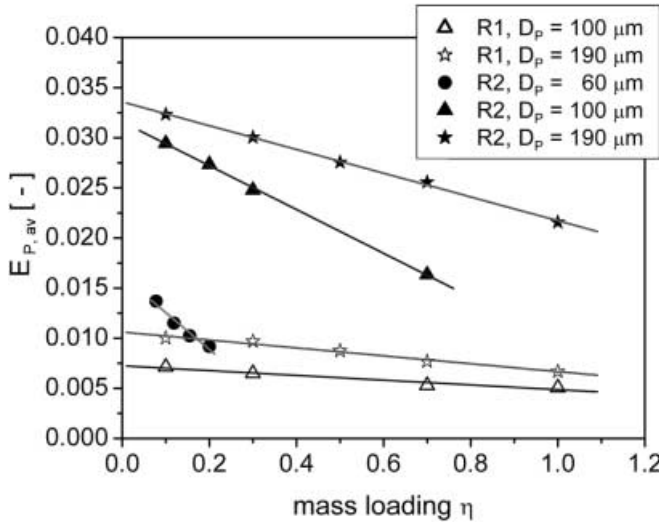

Fig. 14. Particle fluctuation energy averaged across the channel and plotted versus mass loading for different particle diameters and for low (R1) and high (R2) roughness (U_{av}=19.7 m/s)

density c_n for the same loading, whereby the inter-particle collision frequency is enhanced and the particle fluctuation decreases at a higher rate.

With the experimental results obtained, it is now possible also to estimate the importance of inter-particle collisions and wall collisions quantitatively. The mean free path between subsequent collisions λ_C for mono-disperse particles is given according to the kinetic theory of gases by:

$$\lambda_C = \frac{1}{\pi D_p^2 c_n}$$

Introducing the dependence of the number density c_n on the particle volume fraction α_p or the particle mass loading η gives average values of λ_C across the channel:

$$\lambda_C = \frac{D_p}{6\alpha_p} = \frac{D_p}{6\eta}\frac{\rho_p}{\rho}\frac{U_{p,av}}{U_{av}}$$

This result shows that the collision mean free path linearly increases with particle size D_p. For a given mass loading, the mean free path will also depend, in addition to the density ratio ρ_p/ρ, on the ratio of the averaged particle to air velocity $U_{p,av}/U_{av}$. The collision mean free path may now be calculated using the results obtained from the present experiments for low and high roughness (Table 5).

As one would expect, increasing wall roughness decreases the particle average velocity $U_{p,av}$ and therefore, also reduces the mean free path between collisions (the inter-particle collision frequency is increased). For the high roughness and the small particles (60 μm), a loading ratio of 1.0 would result in a mean free path of about 18 mm (estimated, since this condition was not measured) and the corresponding value for 190-μm particles is about 57 mm. These values demonstrate the enormous importance of inter-particle collisions, which will even increase when particle segregation due to gravity takes place. The reduction in the particle number density c_n with increasing size is of course associated with an increase in the mean free path λ_C.

The mean free path between subsequent particle–wall collisions in the horizontal direction λ_W may be estimated by assuming a zig-zag motion of the particle within the channel. This implies that only inertial particles are considered. The mean free path divided by the channel height H is then proportional to the ratio of the cross-sectional averages of the streamwise particle velocity $U_{p,\,av}$ to the relevant particle velocity in the transverse direction:

$$\frac{\lambda_W}{H} = \frac{2U_{p,av}}{|v_{p,rms,av}|}$$

Since the transverse particle velocity distribution involves particles moving upwards and downwards, it is distributed around zero. If we restrict the consideration only to one component, e.g. downward-moving particles, the corresponding transverse mean velocity is roughly half the rms value of the particles, i.e. $v_{p,rms,av}/2$. Using the cross-sectional averages from the measurements, the mean free path associated with wall collisions may be easily estimated. The results for the low and high roughness are summarised in Table 6 and allow the following conclusions:

- With increasing particle size, λ_W is reduced, since the particle motion becomes increasingly wall-collision-dominated, which is also reflected in growing transverse fluctuating velocities.
- The increase in mass loading is associated with an increase in inter-particle collision frequency which causes a reduction in the particle fluctuating velocities and increases λ_W (the wall collision frequency is reduced).
- A reduction in wall roughness decreases the transverse particle velocity fluctuation $v_{p,rms}$ and thereby the mean free path between wall collision is increasing.

Table 5. Dependence of mean free path between subsequent inter-particle collisions on particle diameter and mass loading obtained with the averaged value (across the channel) of the measured particle mean velocity $U_{p,av}$ (– indicates cases which were not measured)

Particle nominal diameter (μm)	Mean free path inter-particle collisions, high roughness (R2) (m)		Mean free path inter-particle collisions, low roughness (R1) (m)
	η = 0.1	η = 1.0	η = 1.0
60	0.182	0.018 (estimated)	–
100	0.313	0.033	0.034
190	0.58	0.057	0.062
625	–	–	0.139

Table 6. Dependence of mean free path between subsequent particle–wall collisions on particle diameter and mass loading obtained with the average value (across the channel) of the measured lateral particle rms velocity fluctuation $v_{p,rms,av}$ (– indicates cases which were not measured)

Particle nominal diameter (μm)	Mean free path particle–wall collisions, high roughness (R2) (m)		Mean free path particle–wall collisions, low roughness (R1) (m)	
	$\eta = 0.1$	$\eta = 1.0$	$\eta = 0.1$	$\eta = 1.0$
60	1.146	–	–	–
100	0.534	0.745	1.298	1.562
190	0.465	0.544	0.896	1.005
625	–	–	–	0.484

These simple estimates provide results which can be used to estimate the importance of inter-particle and wall collisions. Moreover, the estimated wall collision mean free path λ_W was found to be in close agreement with the numerical results for the particle motion in a horizontal channel (submitted, Sommerfeld, 2002).

6 Turbulence modification

The previous results have already shown the well-known effect, namely that small particles will decay fluid turbulence due to the lagging response of the particles with regard to the turbulent fluctuations. This will extract momentum from the fluid and, hence, result in an additional dissipation of turbulence. For larger particles, similar effects occur; however, a large particle Reynolds number will additionally cause wake shedding and, therefore, turbulence intensification may be observed (Tsuji et al. 1984). Crowe (2000) collected extensive data in an attempt to identify the boundary between turbulence dissipation and enhancement. It was argued that the particle mass loading and the ratio of the particle diameter to the turbulence length scale are the relevant parameters for characterisation. However, the flow structure around a particle is governed mainly by the particle Reynolds number.

The results presented in Figs. 6, 7, 10 and 11, clearly showed the reduction in air-phase turbulence mainly in the streamwise fluctuating component with increasing particle loading. The larger particles considered in the experiment, namely 0.625-mm and 1-mm glass beads showed a turbulence enhancement in the core of the channel, which is revealed in Fig. 15 for the streamwise fluctuating component u_{rms}. For the larger particles, this augmentation is of course stronger. In the upper and lower near-wall regions ($y/H<0.3$ and $y/H>0.7$) of the channel, however, a clear turbulence reduction is found. These findings are in agreement with the experiments by Tsuji et al. (1984) and may be directly correlated with the profile of the particle Reynolds number. Since the slip velocity has a maximum in the core of the channel, the particle Reynolds number here reaches values of about 350 and 500 for the 0.625 and 1.0 mm particles, respectively. For these values, the particle wake is characterised by instabilities and wake shedding, which are responsible for turbulence augmentation.

For a further analysis of turbulence modulation, the turbulence spectra were also evaluated for different particle sizes and mass loading using the time series of the streamwise tracer velocity. The calculation of the spectra was performed based on an FFT-technique using the sample-and-hold approach (DANTEC 2001). Eventually, the spectra were smoothed using a Papoulis filter. The minimum frequency in the considered channel was obtained by dividing the rms velocity fluctuation u_{rms} on the centreline by the possible largest dimensions of the eddies, namely the channel height. This gives a value of about 30 Hz. The maximum frequency which can be resolved in

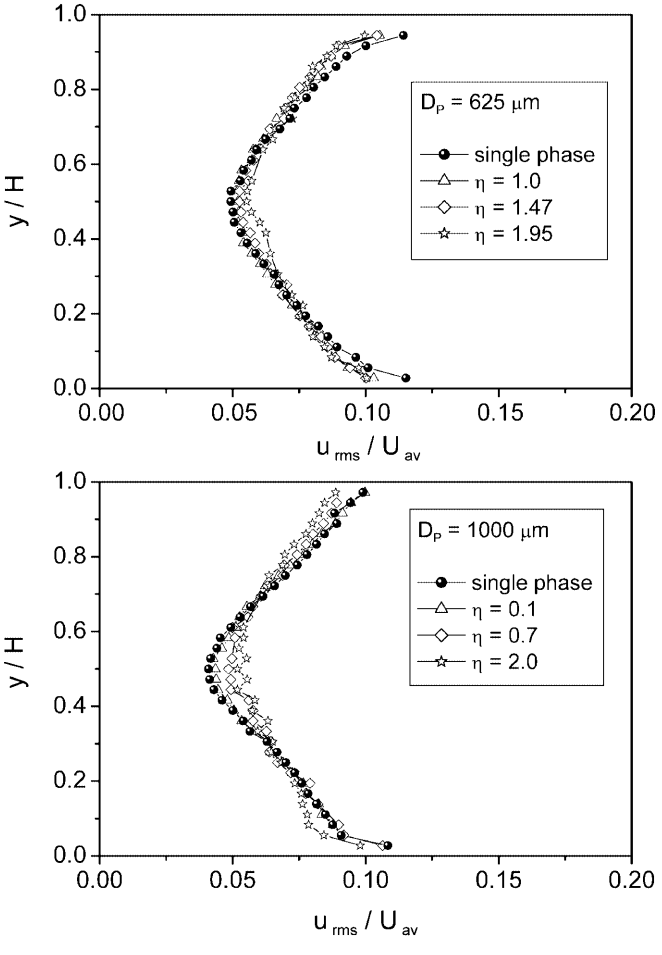

Fig. 15. Profiles for the horizontal component of rms velocity fluctuation comparing different particle diameters for the case of low roughness R1 (U_{av}=19.7 m/s)

the spectrum depends on the signal data rate. For an average minimum value of 8,000 samples/s, the cut-off frequency is about 1,300 Hz. Using additional corrections for interpolation errors and a noise suppression, the spectral estimate is reliable up to frequencies of about 3,000 Hz (Nobach et al. 1998). The estimated Kolmogorov frequency is given by 1,850 Hz according to the time scale provided in Table 1. A typical result for small and large particles is shown in Fig. 16, which was obtained in the centre of the channel. For the 190-μm particles, which caused a considerable reduction in the streamwise air-phase rms velocity fluctuation (u_{rms}) across the entire channel with increasing mass loading η, the spectra reveal a clear reduction in the energy for frequencies above about 50 Hz. The two-phase spectra are parallel to the single-phase result, indicating that turbulence reduction occurred over the entire high-frequency range above 150 Hz.

On the other hand, the spectra of the streamwise air fluctuation u_{rms} for the large particles (625 μm) show a significant increase with mass loading (Fig. 16b). The rate of augmentation is almost constant over the higher frequencies above about 200 Hz. This is consistent with the results obtained in a liquid–solid flow by Sato and Hishida (1996). For most of the cases considered, the slopes for the single-phase flow turbulence spectra are found to be slightly lower than the theoretical value of –5/3 for the inertial subrange. The maximum deviation in the slope was found to be about 8%.

As mentioned before, the turbulence modification should also be affected by wall roughness, since the particle fluctuation is enhanced and the mean transport velocity is decreasing due to the increase in wall collision frequency. Thereby, the slip velocity increases and the momentum transfer between the phases is intensified. This phenomenon is illustrated in Fig. 17, where the non-dimensional streamwise air rms velocity fluctuation averaged across the channel $u_{rms,av}/U_{av}$ is plotted versus the mass loading for different experiments. With increasing particle size, the turbulence dissipation is reduced and eventually, for large particles, wake-generated turbulence becomes dominant and, on average, an augmentation is found for the highest loading considered. For a lower loading, turbulence dissipation dominates, as may be identified from Fig. 15. For the 100-μm and the 190-μm particles, a comparison of results with low and high roughness was possible. These data clearly demonstrate the stronger turbulence decay for higher wall roughness, especially at higher particle mass loading η.

Considering the turbulence spectra for the 100-μm particles in the cases of low and high roughness supports the above observations (Fig. 18). For a higher roughness, the reduction in the energy above about 50 Hz is much more pronounced. This reveals that for higher particle loading, as considered in the present study, the effect of wall roughness cannot be neglected when analysing turbulence modulation. Direct numerical simulations could be very helpful in a further analysis of this effect.

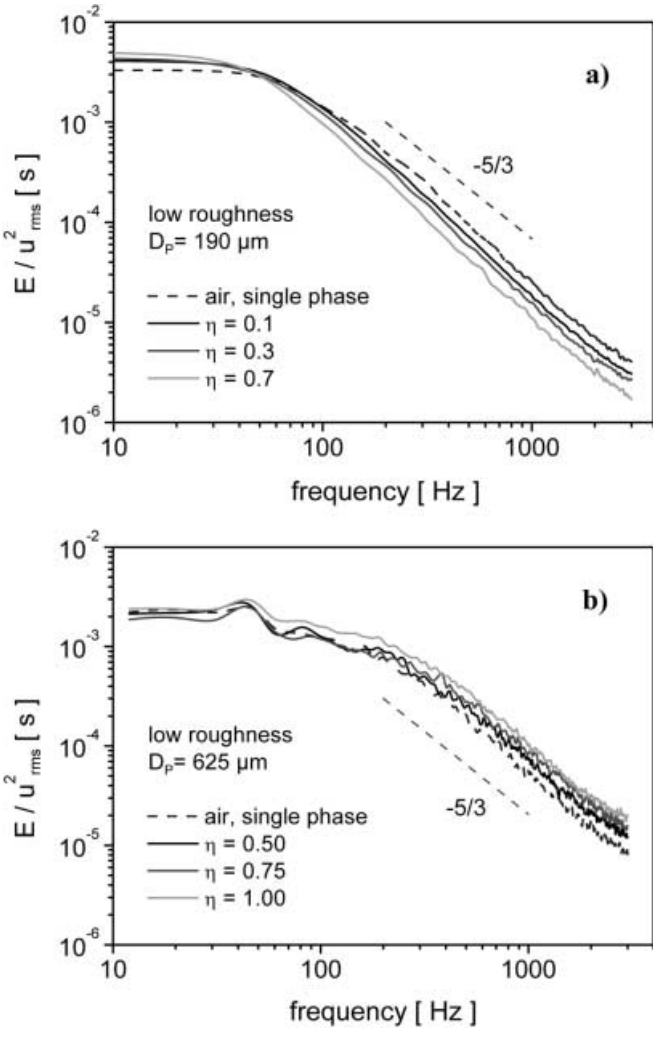

Fig. 16a, b. Normalised turbulence spectra for the horizontal component of air velocities in a gas–particle flow for different particle diameters (U_{av}=19.7 m/s; low roughness R1; centre of the channel): **a** 190 μm; **b** 625 μm

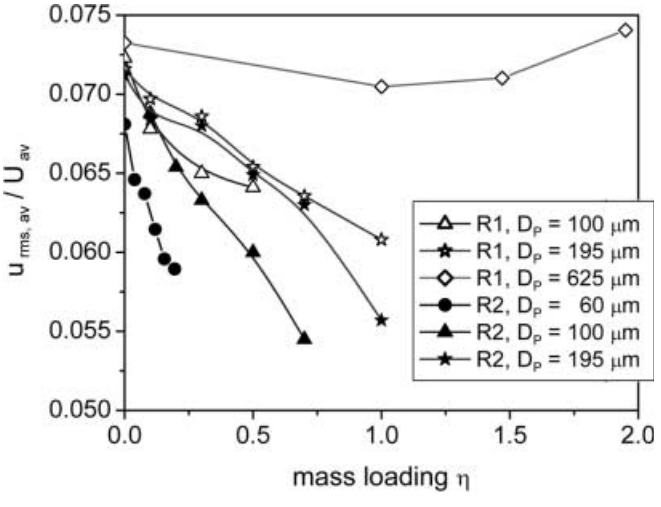

Fig. 17. Normalised horizontal component of gas-phase fluctuating velocity averaged across the channel and plotted versus mass loading for different particle sizes and for low (R1) and high (R2) roughness (U_{av}=19.7 m/s)

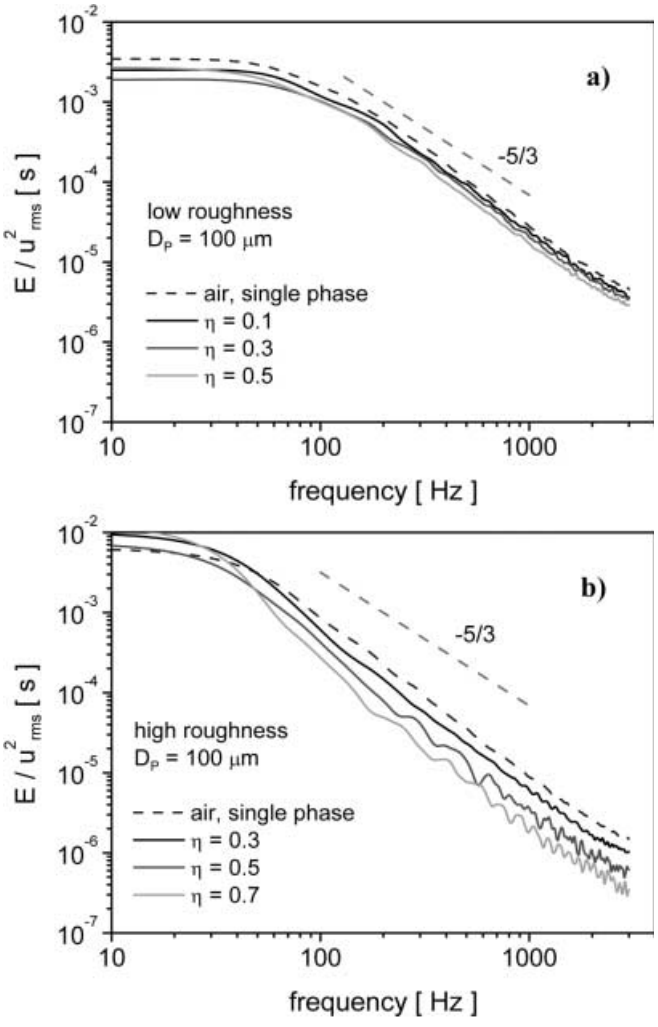

Fig. 18. Normalised turbulence spectra for the horizontal component of air velocities in a gas–particle channel flow with different wall roughness: **a** low roughness; **b** high roughness (U_{av}=19.7 m/s; D_p=100 μm; centre of the channel)

7 Conclusions

Detailed measurements in a particle-laden horizontal channel flow were presented by varying a number of relevant parameters, namely conveying velocity, particle size and mass loading. For the first time, the effect of wall roughness was considered in the examinations. The conveying characteristics of the particles were predominantly affected by their size. With increasing size, the average transport velocity of the particles was reduced. Furthermore, the irregular particle–wall bouncing in case of roughness enhanced the transverse dispersion of the particles across the channel, whereby also the wall collision frequency increased. This was obviously associated with a higher momentum loss for the particle phase, and caused a remarkable reduction in the particle transport velocity $U_{p,av}$. Additionally, both components of the particle rms velocity fluctuation ($u_{p,rms}$ and $v_{p,rms}$) were enhanced due to wall roughness.

With increasing mass loading and hence inter-particle collision frequency, a damping of both fluctuating velocities was observed. This effect was connected with the dissipation of energy associated with an inelastic inter-particle collision process. Moreover, inter-particle collisions improved the transverse dispersion of the particles in the channel. Consequently, gravitational settling was reduced, and the particle concentration profiles became more uniform. In the case of low roughness, low mass loading and small conveying velocity, however, a pronounced gravitational settling of the particles occurred. With increasing mass loading, inter-particle collision frequency increased, and the concentration maximum was shifted from the bottom towards the core of the channel. From the measured data, the inter-particle and wall collision mean free paths (λ_C and λ_W) could be estimated in order to support the main findings of this study.

Finally, the turbulence modulation by small and large particles was analysed. For glass beads with a diameter up to about 200 μm, a pronounced turbulence suppression was found. It could be demonstrated that wall roughness eventually influences turbulence modulation by the particles, as a result of the increased slip velocity between the phases and the enhanced momentum transfer. For a channel with higher wall roughness, this causes a stronger turbulence reduction with increasing mass loading in comparison with a channel with lower wall roughness. For larger particles (0.625 mm and 1.0 mm) turbulence augmentation was restricted to the core of the channel. In the near-wall regions, a reduction in turbulence by the particles was also found.

References

Burmester De Bessa Ribas R, Lourenco L, Riethmuller ML (1980) A kinetic model for a gas–particle flow. Paper presented at Pneumotransport 5, Fifth International Conference on the Pneumatic Transport of Solids in Pipes, London, 16–18 April

Crowe CT (2000) On models for turbulence modulation in fluid–particle flows. Int J Multiphase Flow 26:719–727

DANTEC Measurement Technology (2001) BSA Flow Software, Installation & Users Guide, vol 2. D Dantec Measurement Technology A/S, Skovlunde, Denmark

Gore RA, Crowe CT (1989) Effect of particle size on modulating turbulent intensity. Int J Multiphase Flow 15:279–285

Huber N, Sommerfeld M (1994) Characterization of the cross-sectional particle concentration distribution in pneumatic conveying systems. Powder Technol 79:191–210

Huber N, Sommerfeld M (1998) Modelling and numerical calculation of dilute-phase pneumatic conveying in pipe systems. Powder Technol 99:90–101

Hussain AKMF, Reynolds WC (1975) Measurements in fully developed turbulent channel flow. J Fluids Eng 97:568–580

Kulick JD, Fessler JR, Eaton JK (1994) Particle response and turbulence modification in fully developed channel flow. J Fluid Mech 277:109–134

Matsumoto S, Saito S (1970) On the mechanism of suspension of particles in horizontal pneumatic conveying: Monte Carlo simulation based on the irregular bouncing model. J Chem Eng Jpn 3:83–92

Milojevic D (1990) Lagrangian stochastic-deterministic (LSD) prediction of particle dispersion in turbulence. Part Part Syst Charact 7:181–190

Moin P, Kim J (1982) Numerical investigation of turbulent channel flow. J Fluid Mech 118:341–377

Nobach H, Müller E, Tropea C (1998) Efficient estimation of power spectral density from LDA data. Exp Fluids 24:499–509

Qiu H-H, Sommerfeld M, Durst F (1991) High resolution data processing for phase-Doppler measurements in a complex two-phase flow. Meas Sci Technol 2:455–463

Sato Y, Hishida, K (1996) Transport process of turbulence energy in particle-laden turbulent flow. Int J Heat Fluid Flow 17:202–210
Schlichting H (1965) Grenzschicht-Theorie. G. Braun, Karlsruhe
Sommerfeld M (1992) Modelling of particle–wall collisions in confined gas–particle flows. Int J Multiphase Flow 18:905–926
Sommerfeld M (1996) Modellierung und numerische Berechnung von partikelbeladenen turbulenten Strömungen mit Hilfe des Euler/Lagrange-Verfahrens. Habilitaionsschrift, Universität Erlangen-Nürnberg, Shaker, Aachen
Sommerfeld M (1998) Modelling and numerical calculation of turbulent gas–solid flows with the Euler/Lagrange approach. KONA Powder Particle No. 16:194–206
Sommerfeld M (2000) Theoretical and experimental modelling of particulate flow: overview and fundamentals. Von Karman Institute for Fluid Mechanics Lecture Series No. 2000-6, 1–62.
Sommerfeld M, Huber N (1999) Experimental analysis and modelling of particle–wall collisions. Int J Multiphase Flow 25:1457–1489
Sommerfeld M, Qiu H-H (1995) Particle concentration measurements by phase-Doppler anemometry in complex dispersed two-phase flows. Exp Fluids 18:187–198
Sommerfeld M, Tropea C (1999) Single-point laser measurement. In: Soo SL (ed) Instrumentation for fluid–particle flow, Chap. 7. Noyes Publications, Park Ridge, N.J., pp 252–317
Sommerfeld M, Zivkovic G (1992) Recent advances in the numerical simulation of pneumatic conveying through pipe systems. In: Hirsch Ch, Periaux J, Onate (eds) Computational methods in applied science. Invited lectures and special technological sessions of the First European Computational Fluid Dynamics Conference and the First European Conference on Numerical Methods in Engineering, Brussels, Elsevier Amsterdam, pp 201–212
Tsuji Y, Morikawa Y (1982) LDV measurements of an air-solid two-phase flow in a horizontal pipe. J Fluid Mech 120:385–409
Tsuji Y, Morikawa Y, Shiomi H (1984) LDV measurements of an air-solid two-phase flow in a vertical pipe. J Fluid Mech 139:417–434
Varaksin AY, Kurosaki Y, Satoh I, Polezhaev YV, Polyakov AF (1998) Experimental study of the direct influence of the small solid particles on the carrier air turbulence intensity for pipe flow. In: Proceedings of the 3rd International Conference on Multiphase Flow (ICMF '98), Lyon, France, Paper No. 368
Varaksin AYu, Polezhaev YV, Polyakov AF (1999) Effect of the particles concentration on fluctuating velocity of the disperse phase for turbulent pipe flow. In: Banerjee S, Eaton JK (eds) Turbulence and Shear Flow Phenomena – First International Symposium Santa Barbara, Calif., 12–15 September. Begell House, N.Y.
Yamamoto Y, Potthoff M, Tanaka T, Kajishima T, Tsuji Y (2001) Large-eddy simulation of turbulent gas–particle flow in a vertical channel: effect of considering inter-particle collisions. J Fluid Mech 442:303–334
Zhang Zh, Ziada S (2000) PDA measurements of droplet size and mass flux in the three-dimensional atomisation region of water jet in air cross-flow. Exp Fluids 28:29–35